Mechatronics 000 (2015) 1–10

Contents lists available at ScienceDirect

Mechatronics

journal homepage: www.elsevier.com/locate/mechatronics

Non-singular terminal sliding mode controller: Application to an actuated exoskeleton

T. Madani [a,*], B. Daachi [b], K. Djouani [a,c]

[a] LISSI Lab., University of Paris-Est Creteil, Creteil, France
[b] LIASD Lab., University of Paris 8, Saint Denis, France & CNRS-AIST JRL, UMI 3218/CRT, Tsukuba, Japan
[c] F'SATIE/TUT, Pretoria, South Africa

ARTICLE INFO

Article history:
Received 8 July 2014
Accepted 26 October 2015
Available online xxx

Keywords:
Nonlinear control
Non-singular terminal sliding mode
Finite-time convergence
Exoskeleton

ABSTRACT

This paper presents a robust controller of an active orthosis used for rehabilitation purposes. The system is composed of the orthosis worn by the shank and has a complex dynamical model. No prior knowledge is considered on the dynamical model and the flexion/extension movements considered are of sinusoidal form and are generally defined by the doctor. The used non-singular terminal sliding mode technique permits to have a finite time convergence. The experimental results have been conducted online on an appropriate dummy and then on three healthy subjects. A comparison of performances obtained by the proposed approach with those obtained by a conventional controller has also been realized. Several situations have been considered to test the robustness and it has been concluded with the effectiveness of the developed controller.

1. Introduction

Currently, exoskeletons/orthoses represent a considerable part of robotics research. These wearable robots are used in various fields such as rehabilitation, assistance and can sometimes replace completely the upper or lower limbs of human. In addition, exoskeletons can also be used to improve comfort and help on various daily tasks (gardening, carry heavy loads, climb stairs, walk longer, etc.). Some of main problems considered for this type of robot are related to control, identification of dynamic parameters or behavior and to observe some physical phenomena that can improve exoskeletons performance. Now, the challenge is to improve the cognitive abilities of exoskeletons to enable them to learn, adapt and make decisions based on their own mistakes in the same way than humans. In literature, it can be found several exoskeletons/orthoses developed and used for various applications. The University of Agriculture and Technology of Tokyo has designed an exoskeleton to help the wearer to perform agricultural work considered difficult and tough [7]. Another kind of exoskeleton namely "Hercules" has been made to improve the performance of soldiers.[1] The University of Berkeley has recently developed a lower limb exoskeleton called BLEEX that allows the holder to carry heavy loads [12]. Furthermore, Refs. [4,9] constitute a good state of the art on the exoskeletons and their applications.

To allow the exoskeleton to meet the needs of the wearer, it is necessary to apply an appropriate control law. The complexity of the system dynamics consisting of the exoskeleton and its wearer associated with external perturbations make the traditional controllers inefficient. This complexity has led researchers to propose a variety of appropriate controllers. Some control schemes are based on the preliminary step of identifying the dynamic parameters of the set consisting of the exoskeleton and its wearer. Other approaches are adaptive and are dedicated to generic exoskeletons designed to be worn by humans of different morphologies. An example of such controllers is based on neural networks [10,25]. The universal approximation of neural networks [5,21] is one of their advantages. However, neural approaches require generally offline learning step in order to avoid undesirable behavior of the exoskeleton during the initialization step. In [1], the authors use a dynamical model of the upper limb exoskeleton to amplify the human power. In that human-robot cooperation, it is rarely possible to know the exact dynamical model and consequently the scope of this approach is reduced. Several works on nonlinear control of exoskeletons [8,11] can be also found.

Sliding mode controllers having the advantage of robustness against external disturbances and model uncertainties, have been widely applied to the robotic systems [19,22,23]. The classic sliding mode controllers use a linear sliding surface and the convergence of the system's states is asymptotic. Terminal Sliding Mode (TSM) technique based on a non-linear sliding surface is proposed to ensure, in finite time, the stability of the closed loop system [16,18,20]. The Fast Terminal Sliding Mode (FTSM) surface has been introduced [6,13,26] to further reduce the finite-settling-time. The Non-singular Terminal

* Corresponding author. Tel.: +33 141807335; fax: +33 141807320.
E-mail addresses: tarek.madani@u-pec.fr (T. Madani), bd@ai.univ-paris8.fr (B. Daachi), djouani@u-pec.fr (K. Djouani).

[1] http://www.army-technology.com/features/featurefrench-hercule-robotic-exoskeleton.

http://dx.doi.org/10.1016/j.mechatronics.2015.10.012
0957-4158/

Fig. 1. The dummy and human wearing an actuated knee joint orthosis (EICoSI).

Sliding Mode (NTSM) has been proposed [2,14,15] to overcome the classical singularity problem of the conventional TSM. Furthermore, a boundary layer augmented sliding mode controller is proposed in [3] for trajectory tracking of a robotic orthosis. Even if the obtained results are good, the stability of the system in closed loop is not ensured.

In this article, it is proposed to construct and experiment a NTSM controller for a powered knee orthosis. The goal of the proposed controller is to show the effectiveness of a sliding technique that ensures the convergence toward the sliding surface and avoiding any singularity problem. Surely it can be found other versions of this technique in the literature but as given in the article, it is unique with a particular way to compute the finite time convergence. In fact, a new optimization strategy at the vicinity of the singularity is proposed. This allows to compute the minimum reaching time to the sliding surface. Furthermore, this technique requires no prior knowledge on the dynamic model. Also, the advantage of this method over other methods is its robustness against parameter uncertainties and external disturbances. The system considered in this paper, consisting of the orthosis and knee of the wearer, has a complex dynamic that is difficult to mobilize by equations. For safety reasons, it is very important to control it by techniques including a very short transient tolerated by the standards set by the doctor. This is precisely what offers the NTSM technique that is used in this work. As this technique is almost never used in the field of control of exoskeletons, the presented work proposes a control taking into account the state of the carrier of the exoskeleton that can be active or completely passive (no muscular effort developed). So the proposed controller is firstly tested on an appropriate dummy and is only after eliminating all the risks that application can be made. Final validation is performed on a healthy subject.

The paper is organized as follows: in Section 2, the exoskeleton used for the experiments and formulate the considered problem are described. Section 3 deal with the analysis and controller proposed stability. The experimental results and their analysis are given in Section 4. Finally, Section 5 is dedicated for the conclusion and future work.

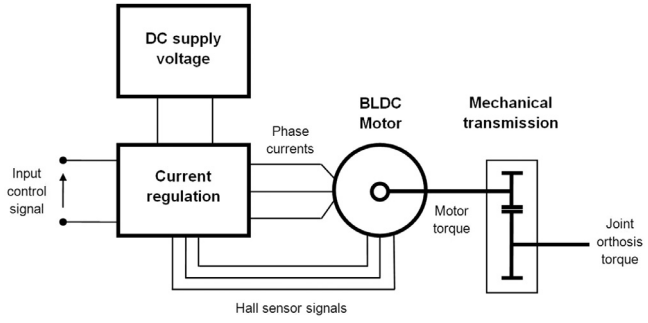

Fig. 2. Electrical architecture of the joint orthosis actuator.

2. Active orthosis system

The EICoSI (Exoskeleton Intelligently Communicating and Sensitive to Intention) is used to carry out the experimental validations of the proposed controller. EICoSI is an active knee-joint orthosis developed in LISSI Laboratory (Laboratoire Images, Signaux et Systèmes Intelligents) of University Paris-Est Créteil (UPEC), France. Two jointed segments compose the considered actuated orthosis, upper and lower. The mechanical part and the actuator are placed on the upper part of the orthosis. The torque generated by the orthosis realizes flexion/extension movements of the lower part, formed by the dummy shank and the lower part of the orthosis. Moreover, the knee joint is constrained by a range of motion between 0 and $\frac{2\pi}{3}$ for safety reason. In Fig. 1, a dummy and a human wearing the used actuated knee joint orthosis are presented.

2.1. Electrical part

The joint of the orthosis is actuated by a brushless DC motor (BLDC). A power supply and an adequate electrical system are used to provide the regulation for the current in the motor. A mechanical

Please cite this article as: T. Madani et al., Non-singular terminal sliding mode controller: Application to an actuated exoskeleton, Mechatronics (2015), http://dx.doi.org/10.1016/j.mechatronics.2015.10.012

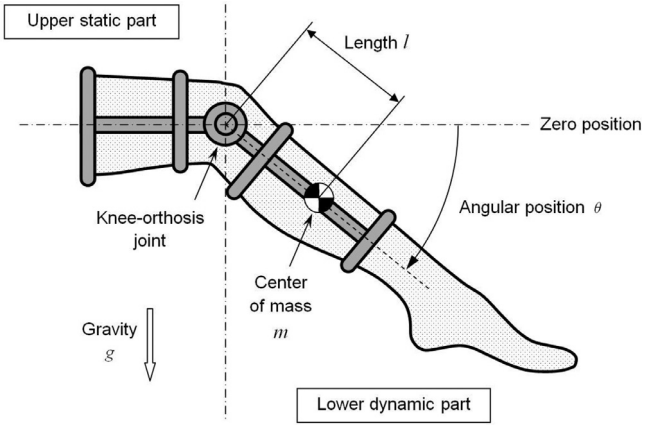

Fig. 3. Position of the joint orthosis.

transmission is used to increase the orthosis applied torque. Fig. 2 shows the schematic diagram of the used electromechanical system.

Assumption 1. The time constant of the electrical system is negligible compared to the mechanical time constant.

According to regulation system characteristics of the BLDC motor and the Assumption 1, the following equation can be written:

$$\tau_a = c_m i \tag{1}$$

where i is the electrical current of the BLDC motor, τ_a is the applied torque and c_m is a positive constant.

2.2. Mechanical part

The mechanical structure scheme of the considered active orthosis is given in Fig. 3. Let θ the angular position of the knee joint-orthosis in the sagittal plane where 0 corresponds to full knee extension and $\frac{\pi}{2}$ rad represents the resting position.

According to the dynamic fundamental principle of solids in rotary motion, it comes:

$$J\ddot{\theta} = \sum \tau_i, \tag{2}$$

where $\ddot{\theta}$ is the angular acceleration, J is the total inertia and τ_i is the applied torques to the knee-orthosis joint for every i.

Assumption 2. The set of joint applied torques in the orthosis are formed by: the actuated orthosis torque τ_a, the human knee joint torque τ_k, the gravitational torque τ_g, the resistive viscous friction torque τ_v, the resistive solid friction torque τ_s and the disturbance torque τ_d which includes all other unmodeled dynamics.

From (2) and Assumption 2, the following dynamic model is obtained where $\dot{\theta}$ is the angular velocity of the knee joint-orthosis and g is the gravitational acceleration:

$$J\ddot{\theta} = \tau_a + \tau_k + \tau_d + \underbrace{mgl\cos(\theta)}_{\tau_g} - \underbrace{k_v\dot{\theta}}_{\tau_v} - \underbrace{k_s sgn(\dot{\theta})}_{\tau_s}, \tag{3}$$

and k_v is the viscous friction coefficient, k_s is the solid friction coefficient, m is the mass and l is the length.

Assumption 3. The parameters $\{J, k_v, k_s, m, l\}$ are unknown, bounded and strictly positive constants.

Assumption 4. The torques τ_k and τ_d are unknown and bounded.

2.3. Dynamic model

The following dynamic model of the whole system is obtained using (1) and (3):

$$\ddot{\theta} = f(\theta, \dot{\theta}, t) + \varphi u(t) \tag{4}$$

with $u = i$ is the electrical current control input, $\varphi = \frac{c_m}{J}$ and the functions $f(\theta, \dot{\theta}, t) \in \mathbb{R}$ is given by:

$$f(\theta, \dot{\theta}, t) = \frac{1}{J}[mgl\cos(\theta) - k_v\dot{\theta} - k_s sgn(\dot{\theta}) + \tau_k(t) + \tau_d(t)] \tag{5}$$

According to Assumptions 3 and 4, it is obvious to write:

$$\begin{cases} \frac{1}{\lambda} \le \varphi \\ |f(\theta, \dot{\theta}, t)| \le a_0 + a_1|\cos(\theta)| + a_2|\dot{\theta}| \triangleq P(\theta, \dot{\theta}) \end{cases} \tag{6}$$

where a_0, a_1, a_2 and λ are adequate positive constants.

One can synthesize the control law forcing the states $\{\theta, \dot{\theta}\}$ of a orthosis to follow the desired trajectory by using the non-singular terminal sliding mode technique.

3. Sliding mode controller design

Our objective is to design a sliding mode control law for the actuated orthosis. The controller generates the control signal $u(t)$ ensuring that the real position $\theta(t)$ tracks the desired one $\theta^d(t)$ in finite-time. This can be done in two main steps:

- Select the NTSM switching manifold so that the system in sliding mode guarantees the convergence to the equilibrium point in finite-time (settling time).
- Determine the control law that guarantees the reachability of the sliding manifold and the appearance of the sliding mode in finite-time (reaching time).

The following lemmas are used to prove the finite time stability of the proposed controller [24]. Their proofs are given respectively in Sections A.1 and A.2 of Appendix A.

Lemma 1. *Let $V(t)$ be a C^1 (continuously differentiable) scalar positive-definite function satisfies the following differential inequality:*

$$\dot{V}(t) \le -\alpha V^{\gamma}(t), \quad \forall t \ge t_0, \quad V(t_0) \ge 0, \tag{7}$$

where $\alpha > 0$ and $0 < \gamma < 1$ are constants. Then, for any given t_0, $V(t)$ checks the following inequality:

$$V^{1-\gamma}(t) \le V^{1-\gamma}(t_0) - \alpha(1-\gamma)(t - t_0), \quad t_0 \le t < t_1, \tag{8}$$

and:

$$V(t) = 0, \quad \forall t \ge t_1, \tag{9}$$

with the finite time t_1 satisfy:

$$t_1 \le t_0 + \frac{V^{1-\gamma}(t_0)}{\alpha(1-\gamma)} \triangleq t^*. \tag{10}$$

Lemma 2. *Let $V(t)$ be a C^1 (continuously differentiable) scalar positive-definite function satisfies the following differential inequality:*

$$\dot{V}(t) \le -\alpha V(t) - \beta V^{\gamma}(t), \quad \forall t \ge t_0, \quad V(t_0) \ge 0, \tag{11}$$

where $\alpha > 0$, $\beta > 0$ and $0 < \gamma < 1$ are constants. Then, for any given t_0, $V(t)$ checks the following inequality:

$$V^{1-\gamma}(t) \le -\frac{\beta}{\alpha} + \frac{\alpha V^{1-\gamma}(t_0) + \beta}{\alpha} \exp^{-\alpha(1-\gamma)(t-t_0)}, \quad t_0 \le t < t_1, \tag{12}$$

and:

$$V(t) = 0, \quad \forall t \ge t_1, \tag{13}$$

with the finite time t_1 satisfy:

$$t_1 \le t_0 + \frac{1}{\alpha(1-\gamma)} \ln \frac{\alpha V^{1-\gamma}(t_0) + \beta}{\beta} \triangleq t^*. \tag{14}$$

Please cite this article as: T. Madani et al., Non-singular terminal sliding mode controller: Application to an actuated exoskeleton, Mechatronics (2015), http://dx.doi.org/10.1016/j.mechatronics.2015.10.012

3.1. Switching manifold selection

Consider the following NTSM switching manifold [14,15]:

$$s \triangleq e + \alpha_s |\dot{e}|^{\gamma_s} sgn(\dot{e}), \tag{15}$$

where $\alpha_s > 0$ and $1 < \gamma_s < 2$ are constants and e is the tracking error defined as:

$$e \triangleq \theta^d - \theta.$$

The used sliding manifold ($s = 0$) guarantees the finite-time convergence of the error e via the following dynamic equation:

$$e = -\alpha_s |\dot{e}|^{\gamma_s} sgn(\dot{e}), \tag{16}$$

Rearranging the last equation yields:

$$\dot{e} = -\alpha_s^{-\frac{1}{\gamma_s}} |e|^{\frac{1}{\gamma_s}} sgn(e). \tag{17}$$

Let t_r be the reaching time to the sliding manifold and assuming that sliding mode is maintained after this time i.e.:

$$s(t) = 0, \quad \forall t \geq t_r. \tag{18}$$

The finite-time convergence of the sliding mode can be proved by the following *Lyapunov* function for the sliding phase:

$$V_s(t) = \frac{1}{2} e^2(t), \quad \forall t \geq t_r, \quad V_s(t_r) \geq 0. \tag{19}$$

Its time derivative is:

$$\dot{V}_s = e\dot{e} = e[-\alpha_s^{-\frac{1}{\gamma_s}} |e|^{\frac{1}{\gamma_s}} sgn(e)] = -\alpha_s^{-\frac{1}{\gamma_s}} |e|^{\frac{1+\gamma_s}{\gamma_s}}. \tag{20}$$

The following equivalent equation is obtained from (20) by replacing $|e|$ by $(2V_s)^{\frac{1}{2}}$:

$$\dot{V}_s = -(\alpha_s^{-\frac{1}{\gamma_s}} 2^{\frac{1+\gamma_s}{2\gamma_s}}) V_s^{\frac{1+\gamma_s}{2\gamma_s}}. \tag{21}$$

According to the Lemma 1, since (21) and the accuracy of the following inequalities:

$$\begin{cases} \alpha_s^{-\frac{1}{\gamma_s}} 2^{\frac{1+\gamma_s}{2\gamma_s}} > 0 \\ 0 < \frac{1+\gamma_s}{2\gamma_s} < 1 \end{cases} \tag{22}$$

then $e(t) = 0$ for $t \geq t_s$ with t_s is the settling time given by:

$$t_s = t_r + \frac{V_s^{1-\frac{1+\gamma_s}{2\gamma_s}}(t_r)}{\alpha_s^{-\frac{1}{\gamma_s}} 2^{\frac{1+\gamma_s}{2\gamma_s}} \left(1 - \frac{1+\gamma_s}{2\gamma_s}\right)}. \tag{23}$$

By using $V_s(t_r) = \frac{1}{2} e^2(t_r)$ and some simplified operations, the settling time t_s can be rewritten as follows:

$$t_s = t_r + \alpha_s^{\frac{1}{\gamma_s}} \frac{\gamma_s}{\gamma_s - 1} \left|e(t_r)\right|^{1-\frac{1}{\gamma_s}}. \tag{24}$$

The elapsed time t_r will be specified in the next section.

3.2. Sliding mode control

The main objective is to generate control law $u(t)$ to achieve and maintain the sliding mode $s = 0$. Thus, the output θ should track the desired trajectory θ^d in finite time, where the trajectory can be an arbitrary function of time.

Let us define the following control law:

$$u = \lambda \left\{ \alpha_r s + sgn(s) \left[\beta_r |s|^{\gamma_r} + P(\theta, \dot{\theta}) + |\ddot{\theta}^d| + \frac{1}{\alpha_s \gamma_s} |\dot{e}|^{2-\gamma_s} + \kappa \right] \right\} \tag{25}$$

with $\alpha_r > 0$, $\beta_r > 0$, $0 < \gamma_r < 1$ and $\kappa > 0$ are constants.

It is easily seen that the control (25) does not contain any terms with negative power due to $1 < \gamma_s < 2$, meaning there will be no singularity.

Theorem 1. *Under the controller (25), the trajectory of the closed-loop system (4) can be driven onto the sliding surface $s(t) = 0$ in a finite time.*

Proof. Consider the following *Lyapunov* function for the reaching phase:

$$V_r(t) = \frac{1}{2} s^2(t), \quad \forall t \geq 0, \quad V_r(0) \geq 0. \tag{26}$$

□

The switching manifold s given in Eq. (15) is continuous and differentiable despite the fact that the signum and absolute value functions are involved (see Section A.3 of Appendix A). So, its derivative with respect to time is:

$$\dot{s} = \dot{e} + \alpha_s \gamma_s |\dot{e}|^{\gamma_s - 1} \ddot{e} \tag{27}$$

By putting (4) in (27) yields:

$$\dot{s} = \dot{e} + \alpha_s \gamma_s |\dot{e}|^{\gamma_s - 1} [\ddot{\theta}^d - f(\theta, \dot{\theta}, t) - \varphi u]. \tag{28}$$

Replacing the control law (25) in (28), one can obtain the following equality:

$$\dot{s} = \dot{e} + \alpha_s \gamma_s |\dot{e}|^{\gamma_s - 1} \left[\ddot{\theta}^d - f(\theta, \dot{\theta}, t) - \varphi\lambda \left\{ \alpha_r s + sgn(s) \times \left(\beta_r |s|^{\gamma_r} + P(\theta, \dot{\theta}) + |\ddot{\theta}^d| + \frac{1}{\alpha_s \gamma_s} |\dot{e}|^{2-\gamma_s} + \kappa \right) \right\} \right] \tag{29}$$

By (29) and (30), the following time derivative of V_r is obtained:

$$\begin{aligned} \dot{V}_r = s\dot{s} = s\{\dot{e} + \alpha_s \gamma_s |\dot{e}|^{\gamma_s - 1} [\ddot{\theta}^d - f(\theta, \dot{\theta}, t)]\} \\ -\lambda\varphi |s| \{ |\dot{e}| + \alpha_s \gamma_s |\dot{e}|^{\gamma_s - 1} [|\ddot{\theta}^d| + P(\theta, \dot{\theta}) + \kappa] \} \\ -\lambda\varphi\alpha_s\gamma_s |\dot{e}|^{\gamma_s - 1} s\{\alpha_r s + \beta_r |s|^{\gamma_r} sgn(s)\}. \end{aligned} \tag{30}$$

From (6), it is easy to verify that $\lambda\varphi \geq 1$ and

$$\begin{aligned} s\{\dot{e} + \alpha_s \gamma_s |\dot{e}|^{\gamma_s - 1} [\ddot{\theta}^d - f(\theta, \dot{\theta}, t)]\} \\ \leq \lambda\varphi |s| \{ |\dot{e}| + \alpha_s \gamma_s |\dot{e}|^{\gamma_s - 1} [|\ddot{\theta}^d| + P(\theta, \dot{\theta}) + \kappa] \} \end{aligned} \tag{31}$$

Therefore $\dot{V}_r$ satisfies:

$$\dot{V}_r \leq -\alpha_s \gamma_s |\dot{e}|^{\gamma_s - 1} (\alpha_r s^2 + \beta_r |s|^{\gamma_r + 1}). \tag{32}$$

Substituting the control (25) into Eq. (4) yields:

$$\ddot{e} = \ddot{\theta}^d - f(\theta, \dot{\theta}, t) - \varphi\lambda \left\{ \alpha_r s + sgn(s) \times \left[\beta_r |s|^{\gamma_r} + P(\theta, \dot{\theta}) + |\ddot{\theta}^d| + \frac{1}{\alpha_s \gamma_s} |\dot{e}|^{2-\gamma_s} + \kappa \right] \right\}, \tag{33}$$

then

$$\begin{aligned} sgn(s)\ddot{e} = sgn(s)\{\ddot{\theta}^d - f(\theta, \dot{\theta}, t)\} - \varphi\lambda\{|\ddot{\theta}^d| + P(\theta, \dot{\theta})\} \\ -\varphi\lambda \left\{ \alpha_r |s| + \beta_r |s|^{\gamma_r} + \frac{1}{\alpha_s \gamma_s} |\dot{e}|^{2-\gamma_s} + \kappa \right\}. \end{aligned} \tag{34}$$

It can be easily seen that Eq. (34) leads to:

$$sgn(s)\ddot{e} < -\kappa \tag{35}$$

Let us use the same reasoning presented in [14,15] to achieve the finite time convergence to the sliding manifold. The inequality (35) suggests that $\dot{e} = 0$ while $e \neq 0$ is not an attractor. For the cases of $s > 0$ and $s < 0$, it yields $\ddot{e} < -\kappa$ and $\ddot{e} > \kappa$ respectively. It means there exists a vicinity of $\dot{e} = 0$, $|\dot{e}|^{\gamma_s - 1} \leq \rho$ for a small positive constant ρ, so that $\ddot{e} < -\kappa$ for $s > 0$ and $\ddot{e} > \kappa$ for $s < 0$ respectively. Therefore the crossing of trajectory from one boundary of the vicinity $\dot{e} = \rho^{\frac{1}{\gamma_s - 1}}$ to the other boundary $\dot{e} = -\rho^{\frac{1}{\gamma_s - 1}}$ for $s > 0$ and from $\dot{e} = -\rho^{\frac{1}{\gamma_s - 1}}$ to $\dot{e} = \rho^{\frac{1}{\gamma_s - 1}}$ for $s < 0$ is finite time t_{r1} such as:

$$t_{r1} \leq \frac{2\rho^{\frac{1}{\gamma_s - 1}}}{\kappa} \tag{36}$$

Please cite this article as: T. Madani et al., Non-singular terminal sliding mode controller: Application to an actuated exoskeleton, Mechatronics (2015), http://dx.doi.org/10.1016/j.mechatronics.2015.10.012

For the region outside the vicinity ($|\dot{e}|^{\gamma_s-1} > \rho$), the following inequality can be written:

$$\dot{V}_r \leq -\alpha_s\gamma_s\rho(\alpha_r s^2 + \beta_r|s|^{\gamma_r+1}). \tag{37}$$

The following equivalent inequality is obtained from (32) by replacing s^2 and $|s|$ by $2V_r$ and $(2V_r)^{\frac{1}{2}}$ respectively:

$$\dot{V}_r \leq -(2\alpha_s\gamma_s\rho\alpha_r)V_r - (2^{\frac{\gamma_r+1}{2}}\alpha_s\gamma_s\rho\beta_r)V_r^{\frac{\gamma_r+1}{2}}. \tag{38}$$

By Lemma 2, since (38) and the coherence of following conditions:

$$\begin{cases} 2\alpha_s\gamma_s\rho\alpha_r > 0 \\ 2^{\frac{\gamma_r+1}{2}}\alpha_s\gamma_s\rho\beta_r > 0 \\ 0 < \frac{\gamma_r+1}{2} < 1 \end{cases} \tag{39}$$

then in the region outside the vicinity ρ, the reaching time t_{r2} to the sliding manifold is given by:

$$\begin{aligned} t_{r2} &\leq \frac{1}{2\alpha_s\gamma_s\rho\alpha_r(1-\frac{1+\gamma_r}{2})} \\ &\times \ln\frac{2\alpha_s\gamma_s\rho\alpha_r V_r^{1-\frac{1+\gamma_r}{2}}(0) + 2^{\frac{\gamma_r+1}{2}}\alpha_s\gamma_s\rho\beta_r}{2^{\frac{\gamma_r+1}{2}}\alpha_s\gamma_s\rho\beta_r} \\ &\leq \frac{1}{\alpha_s\gamma_s\rho\alpha_r(1-\gamma_r)}\ln\frac{\alpha_r|s(0)|^{1-\gamma_r}+\beta_r}{\beta_r} \end{aligned} \tag{40}$$

Therefore, from (36) and (40), the total reaching time from anywhere in the phase plane satisfy the following inequality:

$$t_r \leq t_{r1} + t_{r2} \leq k_1.\rho^{\frac{1}{\gamma_s-1}} + \frac{k_2}{\rho} \triangleq F(\rho) \tag{41}$$

with

$$\begin{cases} k_1 = \frac{2}{\kappa} \\ k_2 = \frac{1}{\alpha_s\gamma_s\alpha_r(1-\gamma_r)}\ln\frac{\alpha_r|s(0)|^{1-\gamma_r}+\beta_r}{\beta_r} \end{cases} \tag{42}$$

The function $F(\rho)$ defined by Eq. (41) represents the upper bound of the reaching time t_r. An optimal choice of ρ allows to minimize the function $F(\rho)$ and then minimize also the reaching time t_r.

Recall that the reaching time t_r is an addition of t_{r1} and t_{r2}, such that:

- The first reaching time t_{r1} is the elapsed time to go out of the vicinity ρ of $\dot{e} = 0$. According to (36) and (42), t_{r1} is bounded by $(k_1\rho^{\frac{1}{\gamma_s-1}}) \triangleq F_1(\rho)$ which is an increasing function according of the variable ρ. This means that in the case of the increasing of the variable ρ then the value of the time t_{r1} increases likewise, and vice versa.
- The second reaching time t_{r2} is the elapsed time to reach on the sliding surface $s = 0$. According to Eq. (40) and (42), t_{r2} is bounded by $(\frac{k_2}{\rho}) \triangleq F_2(\rho)$ which is a decreasing function according to the variable ρ. This means that in the case of the increasing of the variable ρ then the value of the time t_{r2} decreases contrariwise, and vice versa.

Therefore, $F(\rho) = F_1(\rho) + F_2(\rho)$ is a convex downward function according to the vicinity ρ. So, there exists an optimal value of ρ that minimizes the function $F(\rho)$ and the optimum corresponds to the minimum reaching time t_r. Fig. 4 shows an illustrative example with $\gamma_s = 1.5$ and $k_1 = k_2 = 1$.

The function $F(\rho)$ has a minimum which can be easily calculated by solving the equation:

$$\frac{\partial F(\rho)}{\partial\rho} = 0 \tag{43}$$

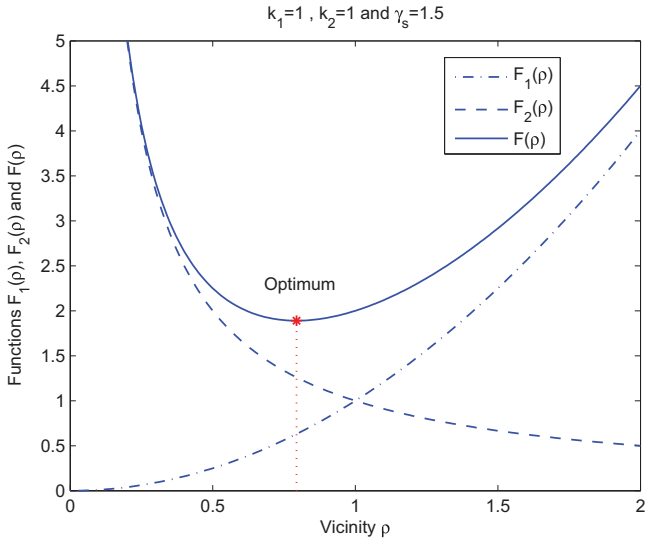

Fig. 4. Illustration example of the vicinity optimization.

After some simple mathematical operations it yields:

$$\rho = \left[\frac{k_2}{k_1}(\gamma_s - 1)\right]^{1-\frac{1}{\gamma_s}} \tag{44}$$

Replacing Eq. (44) in the inequality (41) gives:

$$t_r \leq \gamma_s\left(\frac{k_1}{\gamma_s - 1}\right)^{1-\frac{1}{\gamma_s}} k_2^{\frac{1}{\gamma_s}} \tag{45}$$

This implies that the NTSM is achieved and (18) can be reached in finite-time t_r which is independent of the vicinity ρ.

3.3. Chattering elimination

The sliding mode control signal is discontinuous in nature on the switching manifold. This phenomenon induces a chattering excitation [19] with a very high-frequency oscillation about the sliding surface. Moreover, it may also act as a source that excites the unmodeled high-frequency dynamics of the actuated orthosis. To avoid the effect of this phenomenon, a boundary layer can be used near the sliding surface. One practical solution is to replace the switching function $sgn(s)$ by a saturation function $sat_\delta(s)$, such as:

$$sat_\delta(s) = \begin{cases} sgn(s) & \text{if } |s| > \delta \\ s/\delta & \text{if } |s| \leq \delta \end{cases} \tag{46}$$

where $\delta > 0$ is a small positive constant which characterizes the thickness of the boundary layer.

It is easy to see by using (15) that in the boundary layer $|s| \leq \delta$, if $\dot{e} = 0$ then $|e| < \delta$ and if $e = 0$ then $|\dot{e}| < (\frac{\delta}{\alpha_s})^{\frac{1}{\gamma_s}}$. This gives an evaluation of the loss of precision around the equilibrium point due to the introduction of boundary layer.

4. Experiment results

The purpose of the test is to ensure the good performance of the actuated orthosis to help therapists apply their rehabilitation program in good conditions by using our control strategy. The control law is implemented on a PC equipped with a dSpace DS1103 PPC real-time controller card, using dSpace Control Desk software and Matlab/Simulink. Firstly, the experiment considers a dummy subject weighing 25 kg and measuring 1.70 m (thigh mass = 3 kg, shank mass

Please cite this article as: T. Madani et al., Non-singular terminal sliding mode controller: Application to an actuated exoskeleton, Mechatronics (2015), http://dx.doi.org/10.1016/j.mechatronics.2015.10.012

Table 1
Characteristics of the participating subjects.

Subject	#1	#2	#3
Age (years)	41	39	33
Weight (kg)	73	71	79
Height (m)	1.78	1.69	1.78

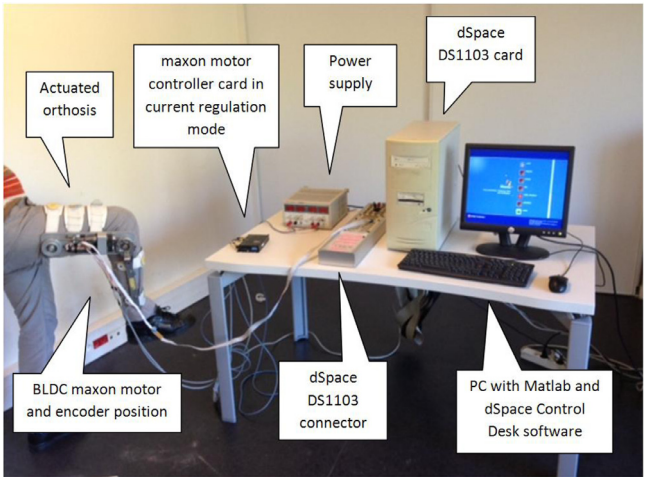

Fig. 5. Experimental setup.

= 2 kg). Secondly, three healthy subjects are selected to the final validation tests. Table 1 gives the characteristics of the participating subjects. Fig. 5 shows our experimental setup.

The sampling time has been fixed to 10^{-3} s. The real position is measured by incremental encoder. A low pass first order filter is used to reduce measurement noise of the angular position.

The controller parameters are fixed at:

$$\alpha_s = 3, \quad , \quad \gamma_s = 1.5,$$
$$\alpha_r = 5, \quad \beta_r = 1, \quad \gamma_r = 0.5,$$
$$a_0 = 2, \quad a_1 = 1.5, \quad a_2 = 0.5,$$
$$\kappa = 0.1, \quad \lambda = 2, \quad \delta = 0.05$$

The considered desired trajectory is sinusoidal with: $\frac{\pi}{4}$ of mean value, $\frac{\pi}{6}$ of amplitude and 1 rad/s of frequency.

For the dummy test, the tracking errors and the switching manifold at $t = 0$ s are:

$$\left.\begin{array}{l} e(0) = -0.13\,\text{rad} \\ \dot{e}(0) = 0.35\,\text{rad/s} \end{array}\right\} \Longrightarrow s(0) = 0.49 \tag{47}$$

Then, the parameters (42) and the vicinity (44) can be calculated:

$$\left.\begin{array}{l} k_1 = 20 \\ k_2 = 0.11 \end{array}\right\} \Longrightarrow \rho = 0.14 \tag{48}$$

This allows us to calculate theoretical reaching and settling time inequalities based on (45) and (24):

$$\begin{cases} t_r \leq 1.19\,s \\ t_s \leq 4.34\,s \end{cases} \tag{49}$$

with the inequality of the settling time t_s is computed by considering $|e(t_r)| \leq |e(0)|$.

In order to evaluate the robustness performances of the proposed approach, a resistive effort $\{\tau_a.\tau_d < 0\}$ and the assistive effort $\{\tau_a.\tau_d > 0\}$ in harmony with the orthosis movement are applied.

Remark: The subject provides an assistive or resistive forces in order to test the robustness of the control law. These disturbances, which must be bounded, are not measurable and their estimation is not needed. Indeed, the proposed control is designed to reject this type of unknown disturbances. The direction of the disturbance is sufficient to know the resistive or assistive nature of the effort useful for illustrations in the figures.

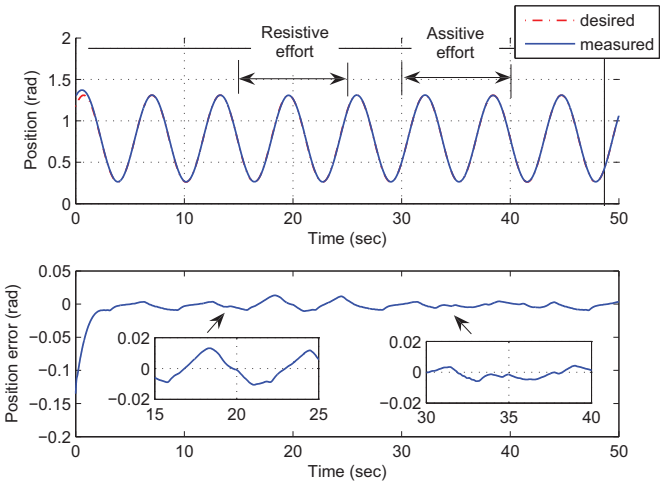

Fig. 6. Measured and desired angular position of the dummy test.

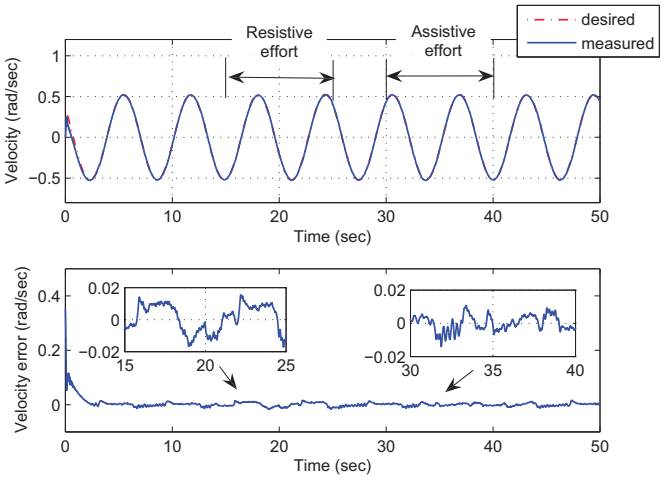

Fig. 7. Measured and desired angular velocity of the dummy test.

The measured and the desired trajectories of the dummy test are given in Figs. 6 and 7. From these figures, it can be seen the good tracking of the trajectories despite the disturbances applied by the subject. The measured trajectories faithfully follow the desired ones even with the resistive or assistive disturbance efforts. On the tracking error figures, the moments of disturbances are zoomed to illustrate their negligible effects.

To show the reaching and settling times of the dummy test, Fig. 8 shows the evolution of the switching manifold s and tracking error e during the beginning of the experiment. It can be noticed that with a consideration of the convergence at ± 5%, the reaching time t_r = 0.2 s and the settling time t_s = 3.5 s which are consistent with the theoretical inequalities (49).

To observe the reaching and the sliding phases in the phase plane of the dummy test, Fig. 9 gives the evolution the tracking error trajectory $\{e, \dot{e}\}$. For the sliding phase, the tracking error is quite similar to that imposed by the sliding surface. The difference between them is justified by the using of the boundary layer (46).

The real current control signal u of the dummy test is shown in Fig. 10. It can be found the good electrical control in both cases with the considered disturbances. The control energy increases if the

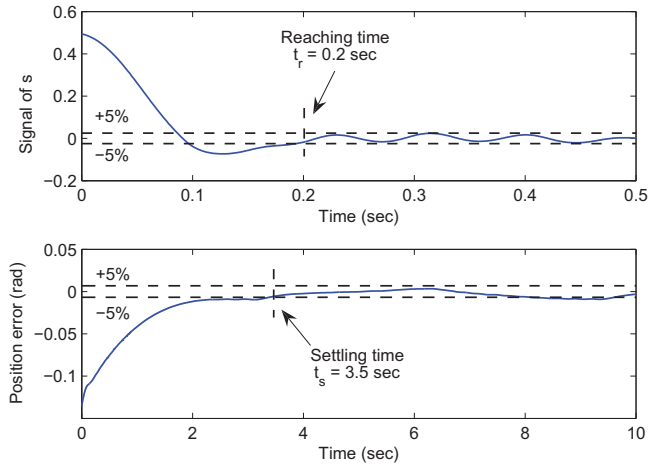

Fig. 8. Reaching and settling times of the dummy test.

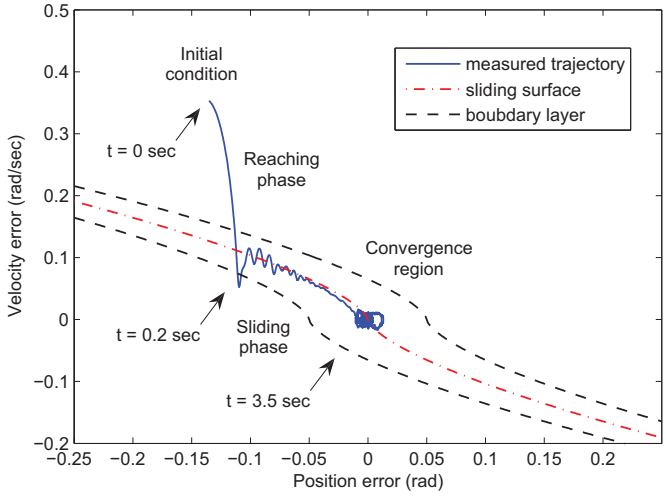

Fig. 9. Reaching and sliding phases in the phase plane of the dummy test.

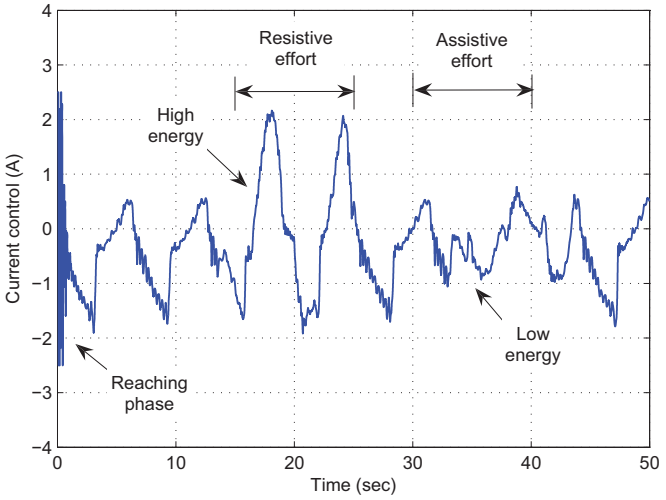

Fig. 10. Control input of the dummy test.

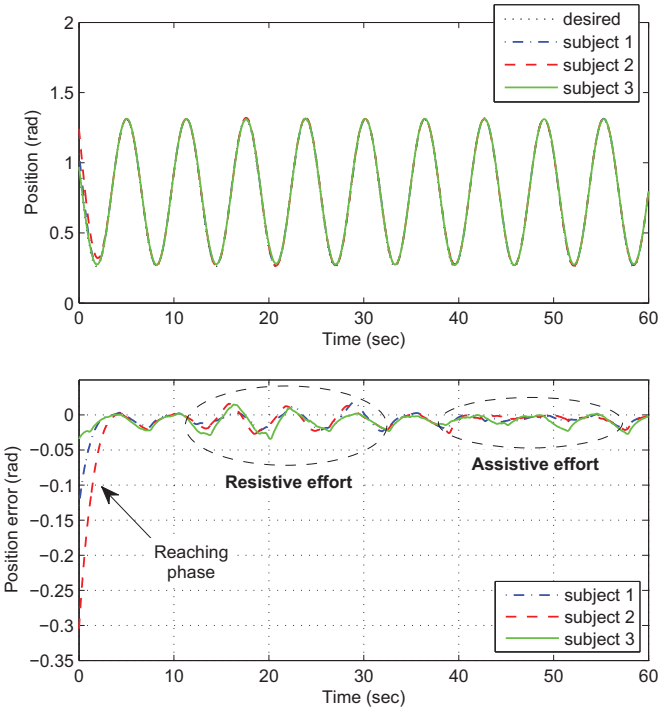

Fig. 11. Measured and desired angular position of the human tests.

disturbance torque is resistive and decreases if otherwise. The control is correct and feasible in practice. The high excitation of the power electrical system is discarded thanks to the chattering phenomenon elimination.

As the results obtained on a dummy are satisfactory, it have been decided to replace the dummy by three healthy subjects (Table 1). The same control parameters used for the dummy are reused for the humans. It have been also used, for the tracking purposes, the same trajectories chosen in the case of the dummy. As shown in Figs. 11–13, it can be noticed good performances in terms of trajectory tracking both in position and in velocity. Furthermore, it can be observed a good behavior of the proposed controller when the human applies a resistive or an assistive effort.

For comparison purposes, it has been applied a Proportional-Integral-Derivative (PID) controller structure given by the following function:

$$u(t) = K_p.e(t) + K_i.\int_0^t e(\tau).d\tau + K_d.\frac{d}{dt}e(t) \tag{50}$$

where K_p is the Proportional gain, K_i is the Integral gain, K_d is the Derivative gain, and τ is the variable of integration takes on values from time 0 to the present time t.

The implementation of the PID controlled is very simple but its design can be difficult because there is no unique method to solve this problem. Indeed, the ideal PID controller does not exist and it should be find a compromise. In general, some specifications are required like stability, robustness, overshoot and settling time of the steady state. The main objective is to bring the process output as close as possible to the desired trajectory and to drive it in a promptly and reliable manner.

Various methods are accordingly used for tuning a PID control loop. There are even sophisticated techniques which are the subject of patents. For our experiment, we used the following tuning method often employed by professionals to obtain the best PID closed loop response. At the beginning, all PID parameters K_p, K_i and K_d are initialized to zero. Firstly, the Proportional gain K_p is adjusted only to have an overshoots of 10–15%. Secondly, the Derivative gain K_d is refined at best the previous passing. Finally, tuned the Integral gain K_i by setting a final overshoots between 5% and 10%. The choice of PID is made heuristically to obtain the best closed loop response. This approximation technique gives us the best (not the optimal) PID parameters. The

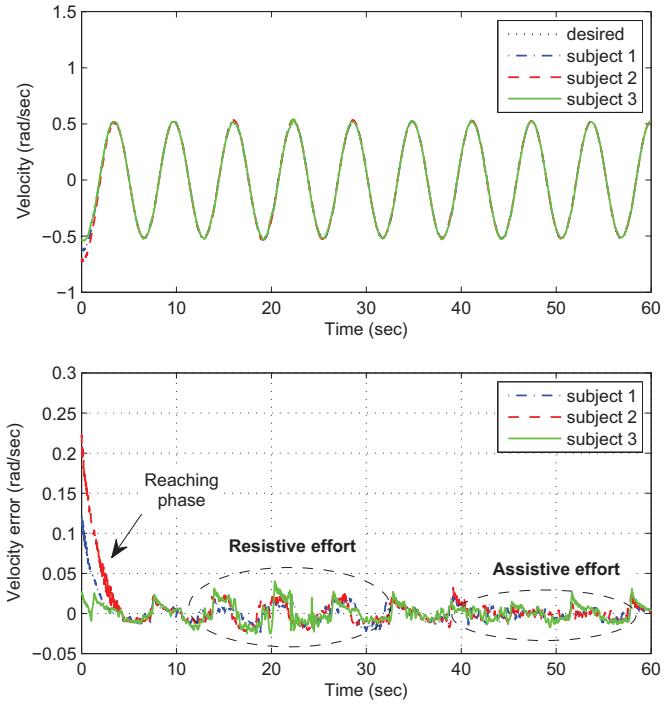

Fig. 12. Measured and desired angular velocity of the human tests.

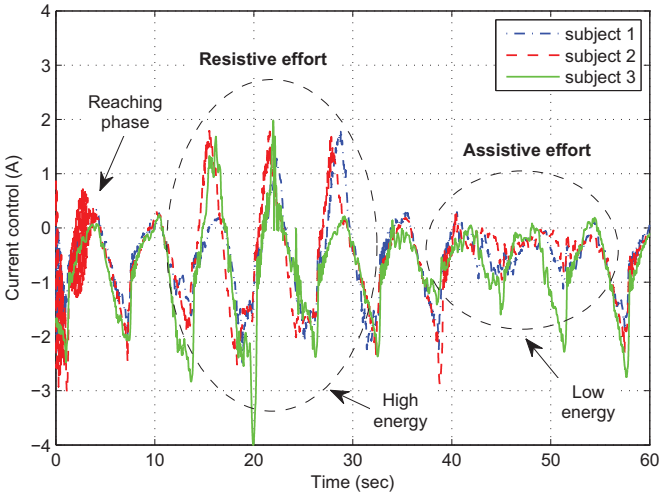

Fig. 13. Control input of the human tests.

selection of the theoretical optimal PID values is very difficult because the exact dynamic model of the real system (the exoskeleton and the human) is unknown. Moreover, the system is strongly nonlinear with an asymmetric behavior (different physical effects depending on the direction of joint motion). In addition, the change of the human subject results in a strong change of the system.

The comparison between controllers are conducted with the subject 1 wearing the actuated knee-orthosis. No muscular effort ($\tau_k = 0$) and no disturbances ($\tau_d = 0$) are applied for this test. Initially, we hoped to test the different controllers with and without external efforts (muscular effort and disturbances). It was not possible to accurately reproduce the same forces on all tested controllers (synchronization and adjusting intensities). Therefore, we had finally presented the results without perturbations in order to compare only the performances in terms of stability.

After a tuning phase, the obtained best values of the PID parameters are $K_p = 10$, $K_i = 5$ and $K_d = 30$. The same NTSM controller

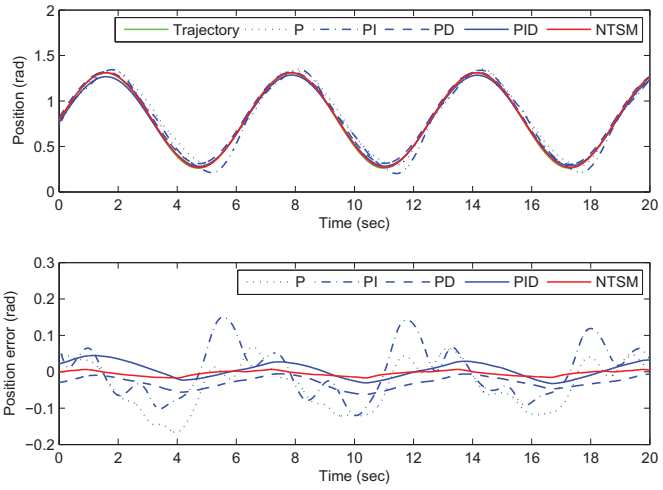

Fig. 14. Comparison between controllers – measured and desired angular positions.

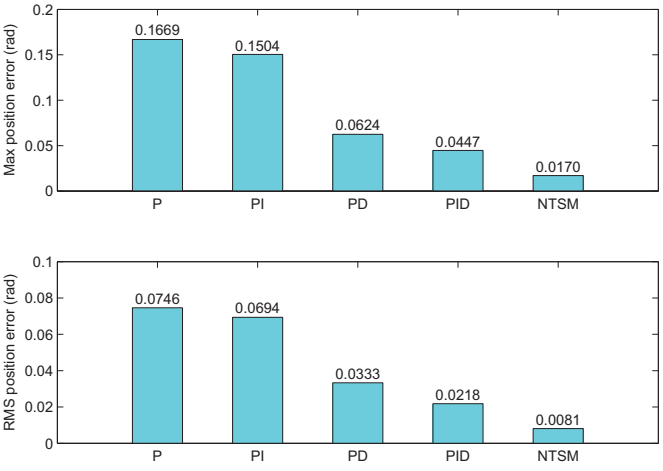

Fig. 15. Comparison between controllers – statistic values of the tracking error.

parameters used for the dummy and the humans in the above studies are also reused here. It is important to note that the selection of the parameters of our NTSM control law was also performed by a manual heuristic method to perform a proper comparison of the tested controllers. The selected best parameters of all used controllers are obtained after several practical tests. After selecting the gains, we noticed the relative simplicity of the NTSM parameter tuning compared to the PID one. This is certainly due to the robustness of the proposed controller.

To perform a multiple test, the controllers P, PI, PD and PID are compared to our NTSM approach. Fig. 14 shows the output positions achieved by the tested controllers. Fig. 15 gives some statistics of the recorded tracking errors where "Max" describes the maximum absolute value computed by $\max_i[|x(t_i)|]$ with t_i is the ith moment ($i = 1, \ldots, n$) and "RMS" is the Root-Mean-Square calculated by $\sqrt{\frac{1}{n}\sum_{i=1}^{i=n} x^2(t_i)}$. It can be clearly found from those results a significant improvement of the proposed NTSM technique in terms of rapidity and accuracy performances. Indeed, the PID provides here satisfactory results but it is well known that this kind of controller is not efficient in case of complex perturbations.

5. Conclusion

This paper developed an efficient controller to ensure good performances desired by the wearer of the orthosis in terms of convergence in a finite time and tolerated by the rules describing the rehabilitation

Please cite this article as: T. Madani et al., Non-singular terminal sliding mode controller: Application to an actuated exoskeleton, Mechatronics (2015), http://dx.doi.org/10.1016/j.mechatronics.2015.10.012

protocol of lower limbs. The proposed controller consists of two steps. In the first step a NTSM switching manifold so that the system in sliding mode guarantees the convergence to the equilibrium point in finite-time (settling time), is selected. The second step aims to determine the control law that guarantees the reachability of the sliding manifold and the appearance of the sliding mode in finite-time (reaching time). The theoretical stability proof of the system in closed loop is ensured according to the *Lyapunov* formalism. Regarding the experimental results, all movements of flexion/extension applied have been conducted smoothly. Furthermore, an ideal behavior of the controller against resistive and assistive muscular efforts applied to the leg of three subjects has been found. For future work, a real application is investigated that can handle a veritable rehabilitation problem with absolute respect of the security protocol that has been defined by the doctor.

Appendix A

A.1. Proof of Lemma 1

Consider the following differential equation:

$$\dot{X}(t) = -\alpha X^{\gamma}(t), \quad \forall t \geq t_0, \quad X(t_0) = V(t_0), \tag{51}$$

where $X(t)$ is a scalar positive-definite function.

It is well known [17] that the solutions $V(t)$ given in (7) and $X(t)$ given in (51) satisfies $V(t) \leq X(t)$ for $t_0 \leq t < t_1$. Therefore the following inequality can be written:

$$V^{1-\gamma}(t) \leq X^{1-\gamma}(t), \quad t_0 \leq t < t_1. \tag{52}$$

Although the differential Eq. (51) does not satisfy the global *Lipschitz* condition, let us proceed to find its unique solution. This equation can be rearranged as:

$$\frac{dX}{dt} = -\alpha X^{\gamma} \Rightarrow -\alpha.dt = X^{-\gamma}.dX \tag{53}$$

Definite integral of the above equation gives:

$$\int_{t_0}^{t} -\alpha.dt = \int_{X(t_0)}^{X(t)} X^{-\gamma}.dX \tag{54}$$

it yields:

$$-\alpha(t - t_0) = \frac{1}{(1-\gamma)}[X^{1-\gamma}(t) - X^{1-\gamma}(t_0)], \tag{55}$$

Since $X(t)$ is a positive-definite function then:

$$X^{1-\gamma}(t) = \begin{cases} X^{1-\gamma}(t_0) - \alpha(1-\gamma)(t - t_0) & \text{if } t_0 \leq t < t^*, \\ 0 & \text{if } t \geq t^*, \end{cases} \tag{56}$$

with

$$t^* = t_0 + \frac{X^{1-\gamma}(t_0)}{\alpha(1-\gamma)}. \tag{57}$$

Finally, by using property (52), formulas (8) and (9) can be written. Fig. 16 shows a graphical representation of the considered finite-time convergence.

A.2. Proof of Lemma 2

Consider the following differential equation:

$$\dot{X}(t) = -\alpha X(t) - \beta X^{\gamma}(t), \quad \forall t \geq t_0, \quad X(t_0) = V(t_0), \tag{58}$$

where $X(t)$ is a scalar positive-definite function.

As previously announced, the solutions $V(t)$ given in (11) and $X(t)$ given in (58) satisfies $V(t) \leq X(t)$ for $t_0 \leq t < t_1$. Therefore the following inequality is satisfied:

$$V^{1-\gamma}(t) \leq X^{1-\gamma}(t), \quad t_0 \leq t < t_1. \tag{59}$$

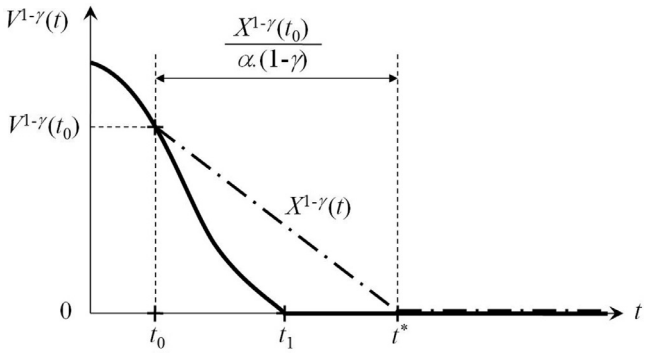

Fig. 16. Finite-time convergence of Lemma 1.

Now, the unique solution of the differential Eq. (58) is studied. This equation does not satisfy the global *Lipschitz* condition and can be rearranged as:

$$X^{-\gamma}\dot{X} + \alpha X^{1-\gamma} = -\beta. \tag{60}$$

By introducing the following variable change:

$$Y = X^{1-\gamma}, \tag{61}$$

its yields:

$$\dot{Y} + AY = B, \tag{62}$$

where

$$\begin{cases} A = +\alpha(1-\gamma) \\ B = -\beta(1-\gamma) \end{cases} \tag{63}$$

The general solution of a first-order linear differential Eq. (62) is:

$$Y(t) = \exp^{-\int_{t_0}^{t} A dt} \left\{ \int_{t_0}^{t} B \exp^{\int_{t_0}^{t} A dt} dt + C \right\}, \tag{64}$$

with $C = Y(t_0)$.Since $Y(t)$ is a positive-definite function then:

$$Y(t) = \begin{cases} \frac{B}{A} + \frac{AC-B}{A} \exp^{-A(t-t_0)} & \text{if } t_0 \leq t < t^*, \\ 0 & \text{if } t \geq t^*, \end{cases} \tag{65}$$

with

$$t^* = t_0 + \frac{1}{A} \ln \frac{AC - B}{-B}. \tag{66}$$

It easy to verify that the above expression of t^* is the same one given in (14).

By using (63), (65) and the change of variable (61), the following expressions can be written:

$$X^{1-\gamma}(t) = -\frac{\beta}{\alpha} + \frac{\alpha X^{1-\gamma}(t_0) + \beta}{\alpha} \exp^{-\alpha(1-\gamma)(t-t_0)}, \quad t_0 \leq t < t^*, \tag{67}$$

and

$$X^{1-\gamma}(t) = 0, \quad \forall t \geq t^*. \tag{68}$$

Finally, (12) and (13) can be written according the property (59). Fig. 17 shows a graphical representation of the considered finite-time convergence.

A.3. Derivative of NTSM switching manifold

The switching manifold (15) can be rewritten as follows:

$$s(e, \dot{e}) = \begin{cases} e + \alpha_s(\dot{e})^{\gamma_s} & \text{if } \dot{e} > 0 \\ e & \text{if } \dot{e} = 0 \\ e - \alpha_s(-\dot{e})^{\gamma_s} & \text{if } \dot{e} < 0 \end{cases} \tag{69}$$

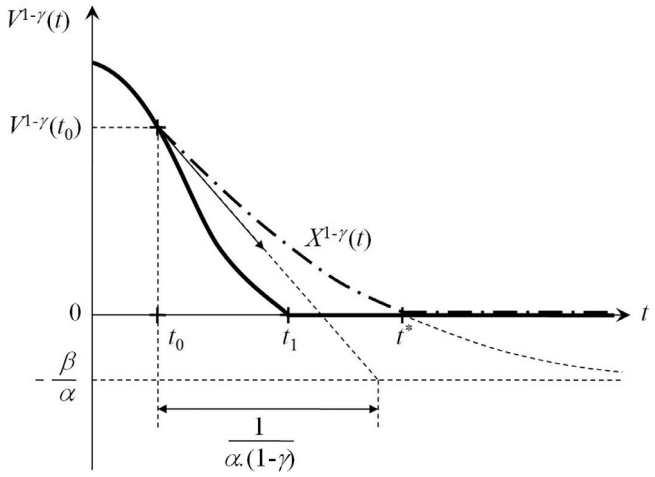

Fig. 17. Finite-time convergence of Lemma 2.

This function is continuous when $\dot{e} > 0$, $\dot{e} < 0$, and it is still continuous at $\dot{e} = 0$ since:

$$s(e,0) = \lim_{\dot{e}\longrightarrow 0^+} s(e,\dot{e}) = \lim_{\dot{e}\longrightarrow 0^-} s(e,\dot{e}) = e. \tag{70}$$

The function $s(e,\dot{e})$ is also differentiable at $\dot{e} = 0$ because we have the partial derivatives at left and right of $\dot{e} = 0$ as:

$$\left.\frac{\partial s(e,\dot{e})}{\partial \dot{e}}\right|_{\dot{e}=0^-} = \lim_{h\longrightarrow 0^-} \frac{\alpha_s(-h)^{\gamma_s}}{-h} = \lim_{h\longrightarrow 0^-} \alpha_s(-h)^{\gamma_s-1} = 0, \tag{71}$$

and

$$\left.\frac{\partial s(e,\dot{e})}{\partial \dot{e}}\right|_{\dot{e}=0^+} = \lim_{h\longrightarrow 0^+} \frac{\alpha_s(h)^{\gamma_s}}{h} = \lim_{h\longrightarrow 0^+} \alpha_s(h)^{\gamma_s-1} = 0. \tag{72}$$

So, the general expression of the partial derivative according to $\dot{e}$ is given by the following system:

$$\frac{\partial s(e,\dot{e})}{\partial \dot{e}} = \begin{cases} \alpha_s\gamma_s(\dot{e})^{\gamma_s-1} & \text{if } \dot{e} > 0 \\ 0 & \text{if } \dot{e} = 0 \\ \alpha_s\gamma_s(-\dot{e})^{\gamma_s-1} & \text{if } \dot{e} < 0 \end{cases}$$

With a simplified formulation, the previous system can be written as:

$$\frac{\partial s(e,\dot{e})}{\partial \dot{e}} = \alpha_s\gamma_s|\dot{e}|^{\gamma_s-1}.$$

Since $\frac{\partial s(e,\dot{e})}{\partial e} = 1$, then the derivative of $s(e,\dot{e})$ with respect to time is given by:

$$\dot{s}(e,\dot{e}) = \frac{\partial s(e,\dot{e})}{\partial e}\dot{e} + \frac{\partial s(e,\dot{e})}{\partial \dot{e}}\ddot{e} = \dot{e} + \alpha_s\gamma_s|\dot{e}|^{\gamma_s-1}\ddot{e}.$$

References

[1] Leea H, Leea B, Kima W, Hanb J, Shinc K, Han C. Human–robot cooperation control based on a dynamic model of an upper limb exoskeleton for human power amplification. Mechatronics 2014;24:168–76.
[2] Komurcugil H. Non-singular terminal sliding-mode control of DC–DC buck converters. Control Eng Pract 2013;21:321–32.
[3] Hussain S, Xie SQ, Jamwal PK. Control of a robotic orthosis for gait rehabilitation. Robot Auton Syst 2013;61:911–19.
[4] Jiménez-Fabián R, Verlinden O. Review of control algorithms for robotic ankle systems in lower-limb orthoses, prostheses, and exoskeletons. Med Eng Phys 2012;34:397–408.
[5] Gomes M, Silveira G, Siqueira A. Gait pattern adaptation for an active lower-limb orthosis based on neural networks. Adv Robot 2011;25(15):1903–25.
[6] Li YQ, Zhou HX, Chen YB. Fast terminal sliding mode control of precision linear motor trajectory tracking system. Control Eng China 2011;18(5):771–4.
[7] Toyama S, Yamamoto G. Development of wearable-agri-robot ˜mechanism for agricultural work. In: Proceedings of IEEE international conference on intelligent robots and systems; 2009. p. 5801–6.
[8] Freeman CT, A-M Hughes JHB, Chappell PH, Lewin PL, Rogers E. Iterative learning control of FES applied to upper extremity for rehabilitation. Control Eng Pract 2009;17(3):368–81.
[9] Dollar AM, Herr H. Lower extremity exoskeletons and active orthoses: challenges and state-of-the-art. IEEE Trans Robot 2008;24(1):144–58.
[10] Aua S, Bernikera M, Herra H. Powered ankle-foot prosthesis to assist level-ground and stair-descent gaits. Neural Netw 2008;21:654–66.
[11] Nef T, Mihelj M, Riener R. Armin: a robot for patient cooperative arm therapy. Med Biol Eng Comput 2007;45:887–900.
[12] Zoss AB, Kazerooni H, Chu A. Biomechanical design of the berkeley lower extremity exoskeleton (BLEEX). IEEE/ASME Trans Mechatron 2006;11(2):128–38.
[13] Yu XH, Man ZH. Fast terminal sliding-mode control design for nonlinear dynamical systems. IEEE Trans Circuits Syst Fundam Theory Appl 2002;49(2):261–4.
[14] Yu X, Zhihong M, Feng Y, Guan Z. Nonsingular terminal sliding mode control of a class of nonlinear dynamical systems. In: Proceedings of 15th triennial world congress of the international federation of automatic control, Barcelona; July 2002.
[15] Feng Y, Yu X, Man Z. Non-singular terminal sliding mode control of rigid manipulators. Automatica 2002;38(12):2159–67.
[16] Man Z, Zu X. Adaptive terminal sliding mode tracking control for rigid robotic manipulator with uncertain dynamic. JSME Int J Ser C 1997;40(3):493–502.
[17] Tang Y. Terminal sliding mode control for rigid robots. Automatica 1998;34(1):51–6.
[18] Man Z, Paplinski AP, Wu HR. A robust MIMO terminal sliding mode control scheme for rigid robotic manipulators. IEEE Trans Automat Control 1994;39:2462–9.
[19] Utkin VI. Sliding modes in control optimization. Berlin, Heidelberg: Springer-Verlag; 1992.
[20] Venkataraman ST, Gulati S. Control of nonlinear systems using terminal sliding modes. In: Proceedings of American control conference; 1989. p. 891–3.
[21] Hornik K, Stinchcomb M, White H. Multilayer feedforward networks are universal approximators. Neural Netw 1989;2:359–66.
[22] Chen C-Y, Li T-HS, Yeh Y-C, Chang C-C. Design and implementation of an adaptive sliding-mode dynamic controller for wheeled mobile robots. Mechatronics 2009;19:156–66.
[23] Utkin VI. Sliding modes and their application in variable structure systems. Moscow: MIR; 1978.
[24] Hale JK. Ordinary deferential equations. Huntington: Krieger; 1969.
[25] Daachi ME, Madani T, Daachi B, Djouani K. A radial basis function neural network adaptive controller to drive a powered lower limb knee joint orthosis. Appl Soft Comput 2015;34:324–36.
[26] Madani T, Daachi B, Djouani K. Finite-time control of an actuated orthosis using fast terminal sliding mode. In: Proceedings of 19th world congress of the international federation of automatic control, Cape Town; August 2014.

Please cite this article as: T. Madani et al., Non-singular terminal sliding mode controller: Application to an actuated exoskeleton, Mechatronics (2015), http://dx.doi.org/10.1016/j.mechatronics.2015.10.012